

THE ROLE OF THE CORE POLARIZATION ON C2 AND C4 FORM FACTORS OF fp -SHELL NUCLEI

FOUAD A. MAJEED^{1,a}, FATIMA M. HUSSAIN²

^{1,2}Department of Physics, College of Education for Pure Sciences, University of Babylon,
P.O. Box 4, Hilla-Babylon, Iraq
E-mail^a: fouadalajeeli@yahoo.com

Received May 2, 2013

Inelastic electron scattering form factors for fp -shell nuclei ^{42}Ca , ^{44}Ca , ^{46}Ti , ^{48}Ti , ^{50}Cr and ^{54}Fe are investigated taking into account higher energy configurations outside the fp -shell. Higher energy configurations, which are called core polarization (CP) effects, are included through a microscopic theory that includes excitations from the core $1s-1p$, $2s-1d$ orbits and also from $2p-1f$ shell to the higher allowed orbits with $6\hbar\omega$ excitations. The calculations are performed in the FP model space by employing GXPF1 and FPD6 effective interactions while the core polarization are calculated with Skyrme-Hartree Fock (Skx) and harmonic oscillator (HO) as residual interactions. The predicated total form factors are compared with the available experimental data and it is shown that the inclusion of the higher excited configuration are very essential in both the transition strength and momentum transfer dependence to obtain reasonable description of the data with no adjustable parameters.

Key words: fp -shell nuclei (e, ϵ), form factors, shell model, calculated first-order core polarization effects.

PACS: 25.30.Dh; 21.60.Cs; 27.40.+z.

1. INTRODUCTION

Nuclear structure models can be successfully tested by comparing the calculated and measured electron scattering form factors [1]. The success of such a model reveals a valuable information about the charge and current distributions of nuclei. We recently used this microscopic calculation [2] in order to study the CP effects on the C2 longitudinal form factors of ^{10}B . Inelastic electron scattering form factors for the excitation of the 2^+ states in the $1f_{7/2}$ nuclei are successfully described in terms of the shell model within the $f_{7/2}^n + f_{7/2}^{n-1} p_{3/2}$ configurations and with the effective interactions [3]. Radhi *et al.* [4–8] have successfully proved that the inclusion of CP effects in the p -shell and sd -shell are very essential to improve the calculations of the form factors. The form factors for the inelastic electron scattering to 2^+ , 4^+ and 6^+ states in $^{46,48,50}\text{Ti}$, $^{50,52,54}\text{Cr}$ and $^{54,56}\text{Fe}$ are studied in the framework of the projected Hartree-Fock model which gave a reasonably good agreement with the experimental form factors using constant effective charges with no adjustable parameters for the calculations of the form factors [9]. Lightbody, Jr. *et al.* [10] measured Rom. Journ. Phys., Vol. 59, Nos. 1-2, P. 95–105, Bucharest, 2014

the elastic and inelastic scattering cross sections for $^{50,52,54}\text{Cr}$ at momentum transfers between 0.5 and 2.6 fm^{-1} along with the comparison between the experimental charge distributions and density dependent Hartree-Fock-Bogolyubov calculations.

The aim of the present work is to study the effect of core polarization on the calculations of $C2$ and $C4$ form factors for some selected states for ^{42}Ca , ^{44}Ca , ^{46}Ti , ^{48}Ti , ^{50}Cr and ^{54}Fe . The core is taken at ^{40}Ca for ^{42}Ca , ^{44}Ca , ^{46}Ti , ^{48}Ti and ^{50}Cr , while ^{48}Ca are taken for ^{54}Fe in the framework of the the fp -shell model. The one body density matrix (OBDM) element used in the present work are calculated by adopting the effective interactions GXPF1 [11] for ^{42}Ca , ^{44}Ca , ^{46}Ti , FPD6 [12] effective interaction is for ^{48}Ti , ^{48}Ca , ^{50}Cr and HO [13] for ^{54}Fe , by generating the wave functions of a given transition in the known nuclei using the modified version of shell model code Oxbash [14]. Higher-energy configurations are included as a first-order core polarization through a microscopic theory which combines shell model wave functions and highly excited states. Transitions from the core $1s-1p$, $2s-1d$ orbits and also from $2p-1f$ orbits to all the higher allowed orbits with excitations up to $6\hbar\omega$ are taking into account. The form factors are calculated without introducing any state dependent parameters such as effective charges, which were introduced in the previous work of authors in this mass region. The CP calculation are performed with Skyrme-Hartree-Fock [15] and harmonic oscillator (HO) potentials as residual interactions. The single-particle wave functions are those of the harmonic-oscillator (HO) potential with size parameter b chosen to reproduce the measured root mean square (rms) charge radii of these nuclei.

2. THEORY

In order to be able to include the CP effects on the form factors microscopically, the shell model wave functions and higher order configurations are combined as first order perturbations. The reduced matrix elements of the electron scattering operator T_Λ is expressed as the sum of the product of the elements of the one-body density matrix (OBDM) $\chi_{\Gamma_f\Gamma_i}^\Lambda(\alpha, \beta)$ times the single-particle matrix elements, and is given by

$$\langle \Gamma_f ||| T_\Lambda ||| \Gamma_i \rangle = \sum_{\alpha, \beta} \chi_{\Gamma_f\Gamma_i}^\Lambda(\alpha, \beta) (\alpha ||| T_\Lambda ||| \beta), \quad (1)$$

where α and β are the final and initial single-particle states for the model space. For fp -shell nuclei, the orbits $1f_{7/2}$, $2p_{3/2}$, $1f_{5/2}$ and $2p_{1/2}$ define the model space. The states $|\Gamma_i\rangle$ and $|\Gamma_f\rangle$ are described by the model space wave functions. Greek symbols are used to denote quantum numbers in coordinate space and isospace, *i.e.* $\Gamma_i \equiv J_i T_i$, $\Gamma_f \equiv J_f T_f$ and $\Lambda = JT$. According to the first-order perturbation theory,

the single-particle matrix element is given by [17]

$$\begin{aligned} \langle \alpha || T_\Lambda || \beta \rangle &= \langle \alpha || T_\Lambda || \beta \rangle + \langle \alpha || T_\Lambda \frac{Q}{E_i - H_0} V_{res} || \beta \rangle \\ &+ \langle \alpha || V_{res} \frac{Q}{E_f - H_0} T_\Lambda || \beta \rangle. \end{aligned} \quad (2)$$

The first term in Eq. (2) is the model space contribution and the second and third terms are the CP contributions. The operator Q is the projection operator onto the space outside the model space. For the residual interaction, V_{res} , we adopt the Skx [15] and HO. E_i and E_f are the energies of the initial and final states, respectively. The CP terms are written as [17]

$$\begin{aligned} &\sum_{\alpha_1, \alpha_2, \Gamma} \frac{(-1)^{\beta + \alpha_2 + \Gamma}}{e_\beta - e_\alpha - e_{\alpha_1} + e_{\alpha_2}} (2\Gamma + 1) \left\{ \begin{array}{ccc} \alpha & \beta & \Lambda \\ \alpha_2 & \alpha_1 & \Gamma \end{array} \right\} \\ &\times \sqrt{(1 + \delta_{\alpha_1 \alpha})(1 + \delta_{\alpha_2 \beta})} \times \langle \alpha \alpha_1 | V_{res} | \beta \alpha_2 \rangle_\Gamma \times \langle \alpha_2 || T_\Lambda || \alpha_1 \rangle \\ &+ \text{terms with } \alpha_1 \text{ and } \alpha_2 \text{ exchanged with an overall minus sign,} \end{aligned} \quad (3)$$

where the index α_1 and α_2 runs over particles states and e is the single-particle energy. The CP parts are calculated by keeping the intermediate states up to the $2p1f$ -shells. The single-particle matrix element reduced in both spin and isospin is written in terms of the single-particle matrix element reduced in spin only [17].

$$\langle \alpha_2 || T_\Lambda || \alpha_1 \rangle = \sqrt{\frac{2T+1}{2}} \sum_{t_z} I_T(t_z) \langle \alpha_2 || T_\Lambda || \alpha_1 \rangle \quad (4)$$

with

$$I_T(t_z) = \begin{cases} 1, & \text{for } T = 0, \\ (-1)^{1/2 - t_z}, & \text{for } T = 1, \end{cases} \quad (5)$$

where $t_z=1/2$ for protons and $-1/2$ for neutrons. The reduced single-particle matrix element of the Coulomb operator is given by [16]

$$\langle \alpha_2 || T_\Lambda || \alpha_1 \rangle = \int_0^\infty dr r^2 j_J(qr) \langle \alpha_2 || Y_J || \alpha_1 \rangle R_{n_1 \ell_1} R_{n_2 \ell_2} \quad (6)$$

where $j_J(qr)$ is the spherical Bessel function and $R_{n\ell}(r)$ is the single-particle radial wave function. Electron scattering form factor involving angular momentum J and momentum transfer q , between the initial and final nuclear shell model states of spin

$J_{i,f}$ and isospin $T_{i,f}$ is [18]

$$|F_J(q)|^2 = \frac{4\pi}{Z^2(2J_i + 1)} \left| \sum_{T=0,1} \begin{pmatrix} T_f & T & T_i \\ -T_z & 0 & T_z \end{pmatrix} \right|^2 \quad (7)$$

$$\times |\langle \alpha_2 || T_\Lambda || \alpha_1 \rangle|^2 |F_{c.m.}(q)|^2 |F_{f.s.}(q)|^2$$

where T_z is the projection along the z-axis of the initial and final isospin states and is given by $T_z = (Z - N)/2$. The nucleon finite-size (f.s) form factor is $F_{f.s.}(q) = \exp(-0.43q^2/4)$ and $F_{c.m.}(q) = \exp(q^2b^2/4A)$ is the correction for the lack of translational invariance in the shell model. A is the mass number, and b is the harmonic oscillator size parameter. The total longitudinal (L) and transverse (T) form factors are given by [16]

$$|F^L(q)|^2 = \sum_{J \geq 0} |F_J^L(q)|^2 \quad (8)$$

$$|F^T(q)|^2 = \sum_{J > 0} \{ |F_J^M(q)|^2 + |F_J^E(q)|^2 \} \quad (9)$$

The total form factor is the sum of the longitudinal and transverse terms [16]

$$|F(q)|^2 = |F^L(q)|^2 + \left[\frac{1}{2} + \tan^2(\theta/2) \right] |F^T(q)|^2 \quad (10)$$

where θ is the electron scattering angle. The single-particle energies are calculated according to [17].

$$e_{nlj} = (2n + l - 1/2)\hbar\omega + \begin{cases} -\frac{1}{2}(l+1)\langle f(r) \rangle_{nl}, & \text{for } j = l - 1/2, \\ \frac{1}{2}l\langle f(r) \rangle_{nl}, & \text{for } j = l + 1/2, \end{cases} \quad (11)$$

with $\langle f(r) \rangle_{nl} \approx -20A^{-2/3}$ and $\hbar\omega = 45A^{-1/3} - 25A^{-2/3}$. The electric transition strength is given by [17]

$$B(CJ, k) = \frac{Z^2}{4\pi} \left[\frac{(2J+1)!!}{k^J} \right]^2 F_J^2(k) \quad (12)$$

where $k = E_x/\hbar c$.

3. RESULTS AND DISCUSSION

The CP effects are calculated with Skx [15] and HO as effective residual interactions. The parameters of the Skx and HO are obtained from the fit to the binding energies, rms charge radii, and single-particle energies. In all of the following diagrams (see figure 1), the dotted curve gives the results obtained using the fp -shell model calculations without CP effects. The results with the inclusion of the CP effects are shown by the dashed curve with Skx as residual interaction and the solid curve are those calculated with HO as residual interaction.

3.1. ^{42}Ca NUCLEUS (1.524 MeV, $J_f^\pi T = 2_1^+ 1$) STATE

The calculations for the $C2$ form factor with full fp -shell wave functions underestimate the data for all q values and the diffractions minimum are shifted to the right compared with the minimum of the measured data as shown by the (dotted curve) in figure 1. The (fp +CP) with Skx describes the measured data very well up to momentum transfer $q \leq 1.5 fm^{-1}$ and start to deviate and overestimate the measured form factor at the second peak. The inclusion of the CP effects enhances the calculations and brings the calculated total form factor near to the measured data and shifts the diffraction minimum to the left, but still can not locate the diffraction minimum at its right location, as shown by the (solid curve) in figure 1. The results of the calculation including the CP effects with Skx as residual interaction gives better description of the form factor than with HO as residual interaction (solid curve) in comparison with the data. The calculation of $B(C2 \uparrow)$ with (fp) is found to be $250 e^2 fm^4$, while the inclusion of the CP effects with Skx as residual interaction predicts the value of $409 e^2 fm^4$ in comparison with the measured value $420 \pm 30 e^2 fm^4$ [19] which is more closer to the measured value than that calculated by [3] as displayed in table 1.

3.2. ^{44}Ca NUCLEUS (1.157 MeV, $J_f^\pi T = 2_1^+ 2$) and (2.283 MeV, $J_f^\pi T = 4_1^+ 2$) STATES

Figure 2 presents the calculation of the $C2$ form factor where the fp -shell model calculation underestimate the experiment and the inclusion of the CP enhances the calculations and brings the form factor to the experimental values in all momentum transfer regions with HO as residual interaction, as shown by the (solid curve) in figure 2. The result of the (fp +CP) calculations is shown by the (dashed curve) where Skx is employed as residual interaction predicts the form factor for the first maximum and starts to deviate in the second and third maximum and overestimates the measured form factor. The $C4$ form factor calculated with fp -shell model calculation underestimate the data at all momentum transfer regions and the locations of the diffraction minimum are slightly displaced to higher q values in comparison to those of the fp -shell model calculations as shown by the (dotted curve) in figure 3. The (fp +CP) for both Skx and HO as residual interactions are agrees reasonably for the first and second maximum. The calculated $B(C2 \uparrow)$ value is found to be equal to $302.2 e^2 fm^4$ (without CP) and $494.4 e^2 fm^4$ (with CP) in comparison with the measured value $470 \pm 20 e^2 fm^4$ [19] and previous theoretical value obtained by [3] as appear in table 1.

3.3. ^{46}Ti NUCLEUS (0.889 MeV, $J_f^\pi T = 2_1^+ 1$) STATE

Figure 4 shows the comparison of the calculated Coulomb $C2$ form factor where the fp -shell model calculation underestimate the experimental data. There

is a significant improvement in the form factors over the fp -shell model results when the CP effects are taken into account with HO as residual interaction and enhances the calculation by a factor of 7.5 and bring it near to the measured data to agrees reasonably up to momentum transfer $q \leq 1.25\text{fm}^{-1}$, but it fails to describe the second maximum. The CP effects with Skx potential are in better agreement with the experimental data than HO as residual interaction, but still underestimate the second maximum in comparison with the measured from factor. fp -model space predicts the value of $B(C2 \uparrow)$ to be $366.3 e^2\text{fm}^4$ which is underestimated the observed value $950 \pm 5 e^2\text{fm}^4$ [19] about 22%, while the (fp +CP) predicts the value of $788.0 e^2\text{fm}^4$ which is also underestimated the measured value about 17% with improvement of 5% over the fp calculations. The inclusion of the CP effects gives a good agreement with the experiment and enhances the $B(C2 \uparrow)$ by a factor of 2.15 over the fp -shell model results and are in better agreement with the value calculated by [3] as tabulated in table 1.

3.4. ^{48}Ti NUCLEUS (0.983 MeV , $J_f^\pi T = 2_1^+ 2$) and (2.42 MeV , $J_f^\pi T = 2_2^+ 2$) STATES

According to the conventional fp -shell model, this nucleus is described taking the core at ^{40}Ca with eight valence nucleons distributed over ($1f_{7/2}$, $2p_{3/2}$, $1f_{5/2}$ and $2p_{1/2}$). The $C2$ form factor for the $J_f^\pi T = 2_1^+ 2$ state at $E_x=0.983 \text{ MeV}$ calculated with fp -shell model wave functions are unable to reproduce the data for all momentum transfer regions (dotted curve) and the inclusion of the CP effects with Skx potential enhance the calculations over the fp -shell model calculations but it overestimates the data for the region of first maximum and underestimates the data in the second region of maximum as shown if figure 5. The calculation of $B(C2 \uparrow)$ with (fp) is found to be $281.3 e^2\text{fm}^4$, while with (fp +CP) with Skx is $766.9 e^2\text{fm}^4$ in comparison with the measured value $720 \pm 40 e^2\text{fm}^4$ [19] as displayed in table 1. The $B(C2 \uparrow)$ calculated by [3] is $665.5 e^2\text{fm}^4$ with underestimation by a factor of 1.08, while our prediction with CP effects included overestimated the measured value by a factor of 1.06. It is very clear that the fp -shell model fails to describe the data in both the transition strength and the form factors.

Figure 6 presents the calculation for the $J_f^\pi T = 2_2^+ 2$ state at $E_x=2.42 \text{ MeV}$. Same comparison are made as in figure 1 and as we can see that the inclusion of the CP effects with Skx as residual interaction gives a better agreement with the experimental value up to momentum transfer $q \leq 1.375 \text{ fm}^{-1}$. Our results agrees with the previous work of [3] where they employed $f_{7/2}^n + f_{7/2}^{n-1} p_{3/2}$ configuration with cal(Ca-Sc) and cal(27-28) as residual interactions.

3.5. ^{50}Cr NUCLEUS (0.783 MeV, $J_f^\pi T = 2_1^+ 1$) and (2.924 MeV, $J_f^\pi T = 2_2^+ 1$) STATES

The core is considered at ^{40}Ca with ten valence nucleons distributed over ($1f_{7/2}$, $2p_{3/2}$, $1f_{5/2}$ and $2p_{1/2}$). The Coulomb $C2$ form factors for the 2_1^+ and 2_2^+ calculations are shown in figures 7 and 8 respectively. The fp -shell model calculations are unable to reproduce the experimental form factors and the inclusion of the CP effects enhance the $C2$ form factors at the first and second maximum and bring the calculated values very close to the experimental data. The locations of the diffraction minimum are correctly reproduced. The $B(C2 \uparrow)$ calculated with fp -shell model is found to be $743.3 e^2 \text{ fm}^4$ in comparison with the measured value $1080 \pm 6 e^2 \text{ fm}^4$ [19] along with the predicted value of $1283.0 e^2 \text{ fm}^4$ from the work of [3] where the residual interaction used was cal(Ca-Sc). Our calculation for $B(C2 \uparrow)$ when the CP effects are included is in better agreement with the observed value than the value calculated by [3] by a factor of 0.93 as displayed in table 1.

3.6. ^{54}Fe NUCLEUS (1.408 MeV, $J_f^\pi T = 2_1^+ 1$) STATE

According to the configuration mixing shell model, ^{54}Fe nucleus is considered as an inert ^{48}Ca core and six valence nucleons distributed over the ($1f_{7/2}$, $2p_{3/2}$, $1f_{5/2}$ and $2p_{1/2}$) orbits. The fp -shell model calculations underestimate the measured data and the location of the minimum are slightly shifted towards high q values. When the CP effects are introduced the data are in excellent agreement with Skx and with HO the first region of maximum are correctly reproduced while the second region of maximum are underestimated. Our results are in better agreement with Skx than those of [3] where their calculations by means of $f_{7/2}^n + f_{7/2}^{n-1} p_{3/2}$ configuration with cal(27-28) are unable to reproduce the second maximum and the location of the minimum are produced in the wrong location and shifted to the high q values. The inclusion of the CP effects enhances the value predicted by fp -shell model calculations, but it overestimated the measured value and it is found to be same order of magnitude of the value predicated by [3] with cal(Ca-Sc) residual interaction as tabulated in table 1.

Table 1

Theoretical values of the reduced transition probabilities $B(C2 \uparrow, k)$ (in units of $e^2 fm^4$) and in comparison with experimental values and other theoretical calculations.

Nucleus	J_f^π	T_f	$E_x(\text{MeV})$	fp	$fp+CP$ Skx	Other [3]	Exp. [19]
^{42}Ca	2_1^+	1	1.524	250.0	409.0	395.0	420 ± 30
^{44}Ca	2_1^+	2	1.157	302.2	494.4	491.5	470 ± 20
^{46}Ti	2_1^+	1	0.889	366.3	788.0	649.5	950 ± 5
^{48}Ti	2_1^+	2	0.983	281.3	766.9	665.5	720 ± 40
^{50}Cr	2_1^+	1	0.783	734.3	1197.0	1283.0	1080 ± 6
^{54}Fe	2_1^+	1	1.408	431.5	902.0	915.5	620 ± 5

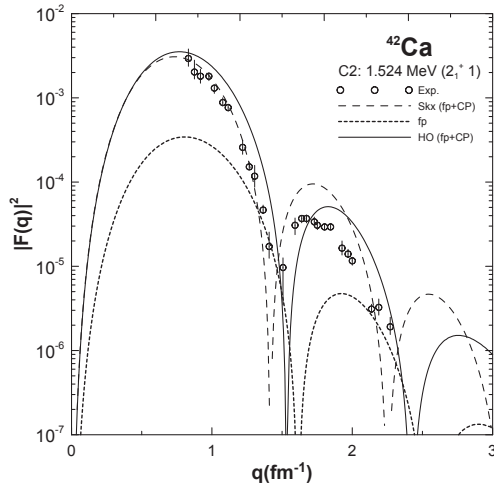


Fig. 1 – The Coulomb form factor of the quadrupole transition $2_1^+ 1$ (1.524 MeV) in ^{42}Ca . The data are taken from [20].

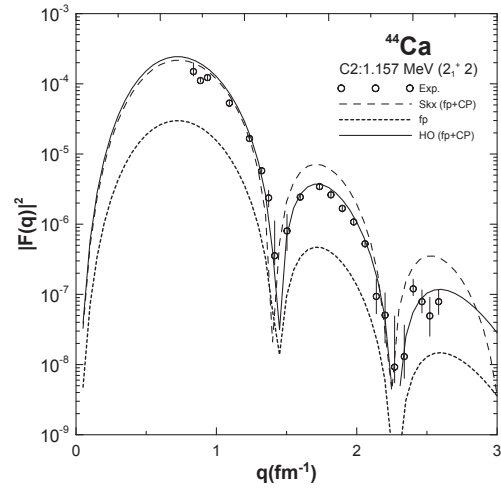


Fig. 2 – The Coulomb form factor of the quadrupole transition $2_1^+ 2$ (1.157 MeV) in ^{44}Ca . The data are taken from [20].

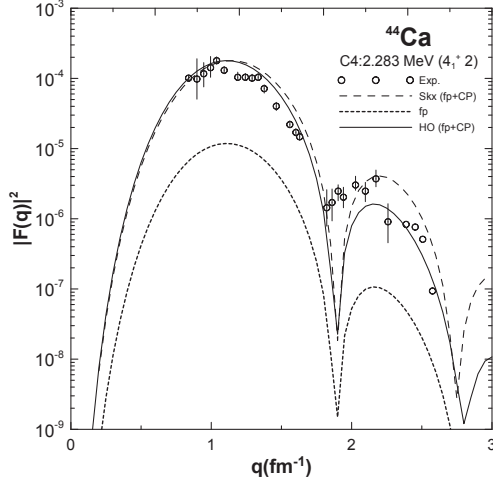


Fig. 3 – The Coulomb form factor of the hexadecupole transition $4_1^+ 2$ (2.283 MeV) in ^{44}Ca . The data are taken from [20].

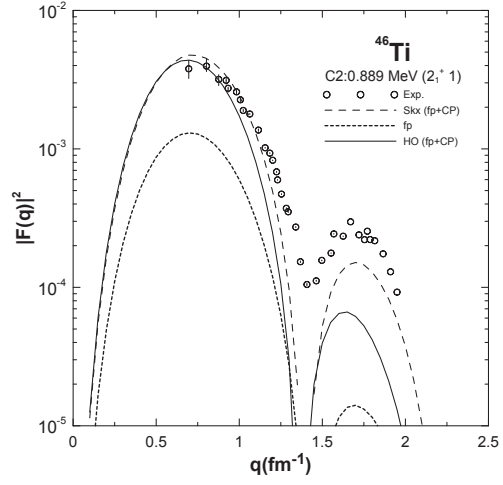


Fig. 4 – The Coulomb form factor of the quadrupole transition $2_1^+ 1$ (0.889 MeV) in ^{46}Ti . The data are taken from [20].

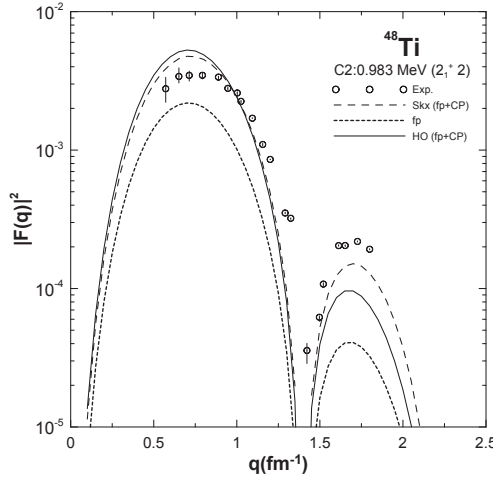


Fig. 5 – The Coulomb form factor of the quadrupole transition $2_1^+ 2$ (0.983 MeV) in ^{48}Ti . The data are taken from [21] and [22].

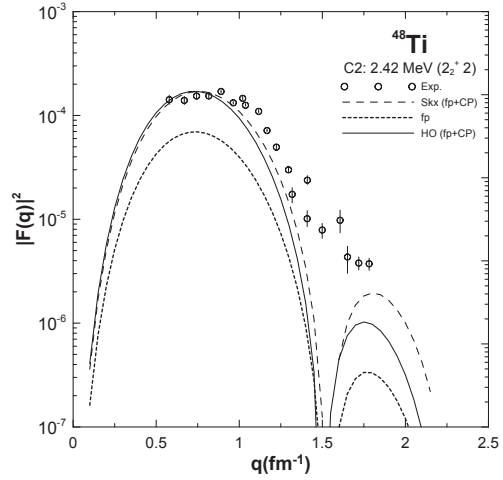


Fig. 6 – The Coulomb form factor of the quadrupole transition $2_2^+ 2$ (2.42 MeV) in ^{48}Ti . The data are taken from [21] and [22].

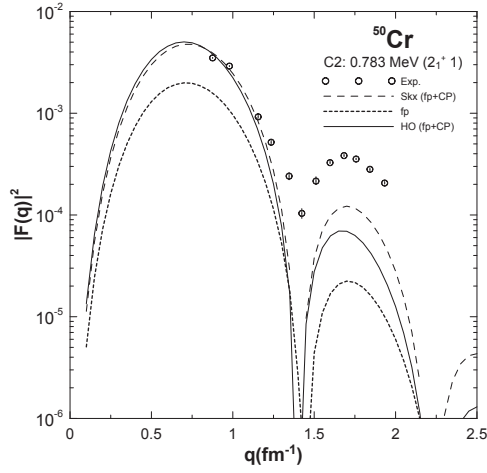


Fig. 7 – The Coulomb form factor of the quadrupole transition 2_1^+ (0.783 MeV) in ^{50}Cr . The data are taken from [10].

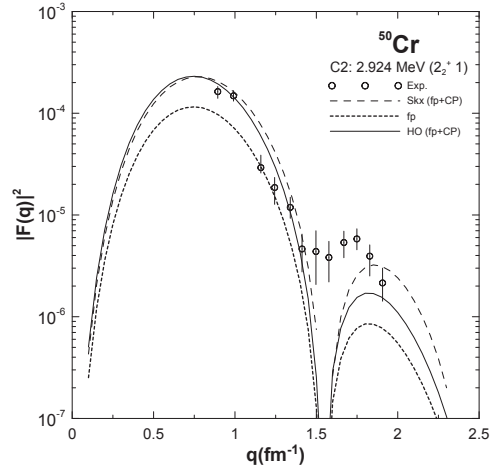


Fig. 8 – The Coulomb form factor of the quadrupole transition 2_2^+ (2.924 MeV) in ^{50}Cr . The data are taken from [10].

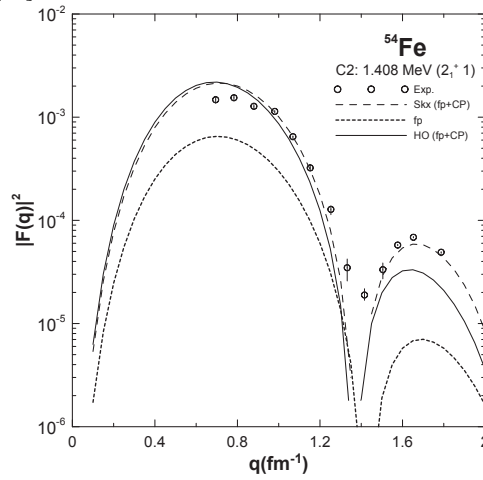


Fig. 9 – The Coulomb form factor of the quadrupole transition 2_1^+ (1.408 MeV) in ^{54}Fe . The data are taken from [22].

4. CONCLUSIONS

A conclusion were drawn that the inclusion of the CP effects are found to be very essential in the calculations of the $C2$ and $C4$ form factors and gives remarkably good agreement over the fp -shell model calculations for the form factors and the absolute strengths. The fp -shell models, are able to predicts the static properties and energy levels of nuclei lies in the fp -shell region but it had shortfall in describing the dynamic properties such as $C2$ transition rates and electron scattering form factors. The choice of Skx as residual effective interaction are more adequate than HO for core polarization calculations. The inclusion of higher-excited configurations by means of CP enhances the form factors and brings the theoretical results closer to the experimental data. These calculations can be extended to cover the entire fp -shell region depending on the availability of the experimental data, and also can be used even for higher shells.

REFERENCES

1. F.A. Majeed and R.A. Radhi, Chinese Phys. Lett. **23**(10), 2699–2702 (2006).
2. F.A. Majeed, Phys. Scr. **85**(6), 065201–065205 (2012).
3. T. Iwamoto, H. Horie and A. Yokoyama, Phys. Rev. C **25**, 658–666 (1982).
4. R.A. Radhi, A.A. Abdullah, Z.A. Dakhil, N.M. Adeeb, Nucl. Phys. A **696**, 442–452 (2001).
5. R.A. Radhi, Nucl. Phys. A **707**, 56–64 (2002).
6. R.A. Radhi, Eur. Phys. J. A **16**, 381–385 (2003).
7. R.A. Radhi, Nucl. Phys. A **716**, 100–106(2002).
8. R.A. Radhi, Eur. Phys. J. A **16**, 387–392 (2003).
9. R. Sahu, K.H. Bhatt and D.B. Ahalparas, J. Phys. G: Nucl. Part. Phys. **16**(5), 733–743 (1990).
10. J.W. Lightbody, Jr. *et al.*, Phys. Rev. C **27**, 113–132 (1983).
11. M. Honma, T. Otsuka, B.A. Brown, T. Mizusaki, Phys. Rev. C **65**, 061301(R)–061306(R) (2002).
12. W.A. Richter, M.G. Van der Merwe, R.E. Julies, B.A. Brown, Nucl. Phys. A **523**, 325–353 (1991).
13. H. Horie and K. Ogawa, Prog. of The. Phys. **46**, 439–461 (1971).
14. Oxbash for Windows, B.A. Brown, A. Etchegoyen, N.S. Godwin, W.D.M. Rae, W.A. Richter, W.E. Ormand, E.K. Warburton, J.S. Winfield, L. Zaho, C.H. Zimmerman, MSUNSCL, report number **1289** (2004).
15. B.A. Brown, Phys. Rev. C **58**, 220–231 (1998).
16. T. de Forest Jr., J.D. Walecka, Adv. Phys. **15**, 1–109 (1966).
17. P.J. Brussaard, P.W.M. Glaudemans, *Shell-Model Applications in Nuclear Spectroscopy* (North Holland Publ. Co., Amsterdam, 1977).
18. T.W. Donnelly, I. Sick, Rev. Mod. Phys. **56**, 461–566 (1984).
19. S. Raman, C.W. Nestor, Jr., and P. Tikkanen, At. Data Nucl. Data Tables **78**, 1–128 (2001).
20. J. Heisenberg, J.S. McCarthy, and I. Sick, Nucl. Phys. A **164**, 353–366 (1971).
21. A. Hotta, K. Hayakawa, K. Takayama, I. Okazaki, and M. Oyamada, Res. Rep. Nucl. Sci. (Tohoku Univ.) **9**, 7 (1976); **10**, 18 (1977).
22. K. Hosoyama, A. Hotta, M. Kawamura, T. Nakazato, and M. Oyamada, Res. Rep. Nucl. Sci. (Tohoku Univ.) **11**, 1 (1978).